Wed-Af-Po.12-01

Conduction Cooled Cryogenic Current Drive with HTS Filter

Vyacheslav Solovyov, Mustafeez Hassan, Yuxuan Wu (吴宇轩), and Paul Farrell

***Abstract*— We propose and demonstrate an in-vacuum synchronous rectifying DC current drive with no thermal linkage between room temperature and cryogenic environments. The high-voltage signal is stepped down by an array of in-vacuum transformers and converted to DC by a cryogenic synchronous rectifier circuit, designed to handle a maximum current of 700 A. The key component of the current drive is an HTS filter, which ensures < 50 mV voltage ripple on the load. We discuss the design of the filter inductance and identify off-shelf capacitors that can operate below 20 K. We analyze the source of both conduction and switching losses. The conduction losses are shown to dominate the thermal load on the cryogenic side. Proper management of the conduction and switching loss thus enables design of a conduction-cooled HTS magnet system rated for 1,000 A capacity that is cooled with a single-stage cryocooler. The source operation is demonstrated on a second-generation HTS magnet operating at 18 K.**

***Index Terms*— High-temperature superconductors, power supplies, current leads, superconducting magnets.**

I. INTRODUCTION

Traditionally, the current is delivered to a superconducting magnet through a normal metal lead. Fig. 1a presents a schematic of the conventional current delivery architecture for superconducting magnets. In this configuration, a high-voltage signal is initially stepped down by a transformer, followed by rectification and low-pass filtering. The resulting high-current DC output is then supplied to the magnet via cryogenically cooled current leads. These leads are thermally managed using a combination of thermal intercepts, cryogen vapor cooling, or direct immersion in liquid cryogens [1]. The intricate design and implementation of thermal intercepts contribute substantially to the overall cost of the current leads—often exceeding the cost of the magnet itself. The widely accepted normal metal current lead optimization methodology has been developed by McFee [2]. Due to the limitations imposed by the Wiedemann-Franz law, the minimum loss is independent of the lead material and is ≈ 45 W per 1,000 A of DC current. The second-generation (2G) high-temperature superconductors (HTS) are now extensively used to deliver DC current from 77 K and below, but normal metals are still used to cover the span from room temperature to 77 K [3, 4], often requiring complex liquid Nitrogen coolers [5].

So-called exciters [6] and flux pumps [7] are often used to inject current into a magnet wirelessly by subjecting a section of the conductor to a changing magnetic field. These devices are capable of generating only small (tens of millivolt) voltage on a coil and operate in a pulsed (topping-off) mode.

As previously reported [8], operating n-type silicon MOSFETs at cryogenic temperatures between 50 K and 60 K leads to a decrease in channel resistance by approximately a factor of two. In modern high-performance devices, such resistance values fall well below 1 mΩ per unit, thus making possible design of low-loss cryogenic rectifiers and flux pumps

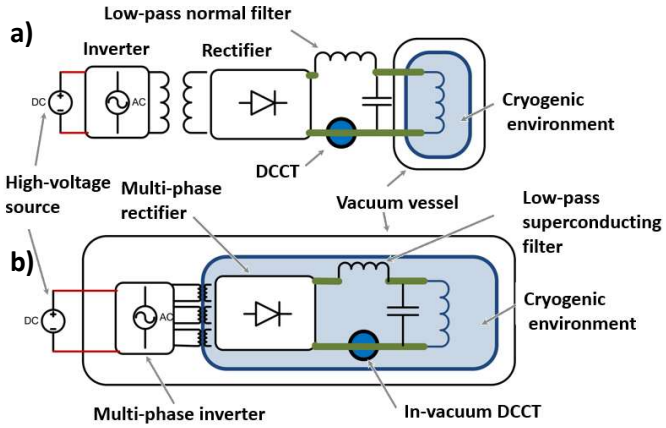

Fig. 1. a) Traditional current control of a superconducting magnet. b) Current source based on an in-vacuum cryocooled synchronous rectifier and filter.

by parallel connection of multiple MOSFETS [9], [10]. However, switching semiconductor rectifiers inherently introduce voltage ripple, reaching amplitudes in the range of several hundred millivolts. Mitigation of high-frequency voltage ripple via a high-current *LC* filter is critical for the practical implementation of a superconducting magnet current source. In the proposed cryogenically cooled, in-vacuum architecture (Fig. 1b), the primary electrical power is introduced into the cryogenic vacuum chamber as a high-voltage, low-current DC signal through a compact vacuum feedthrough. This signal is subsequently stepped down inside the cryo-chamber by an array of phase-shifted inverters and transformers. The output is then rectified using synchronous rectifiers and further conditioned by an HTS *LC* filter,

Manuscript received ; accepted . Date of publication; date of current version . This work was supported by U.S. DOE Office of Science award DE-SC0013856. *(Corresponding author: Vyacheslav Solovyov.)*

V. F. Solovyov is with Brookhaven Technology Group, 1000 Innovation Road, Stony Brook, NY 11794, (slowa@brookhaventech.com).

Paul Farrell is with Brookhaven Technology Group, 1000 Innovation Road, Stony Brook, NY 11794 (pfarrell@brookhaventech.com).

Mustafeez Hassan and Yuxuan Wu are with Stony Brook University, Stony Brook, NY 11794 (mustafeez.hassan@stonybrook.edu, yuxuan.wu@stonybrook.edu).

Color versions of one or more of the figures in this paper are available online at http://ieeexplore.ieee.org.

Digital Object Identifier

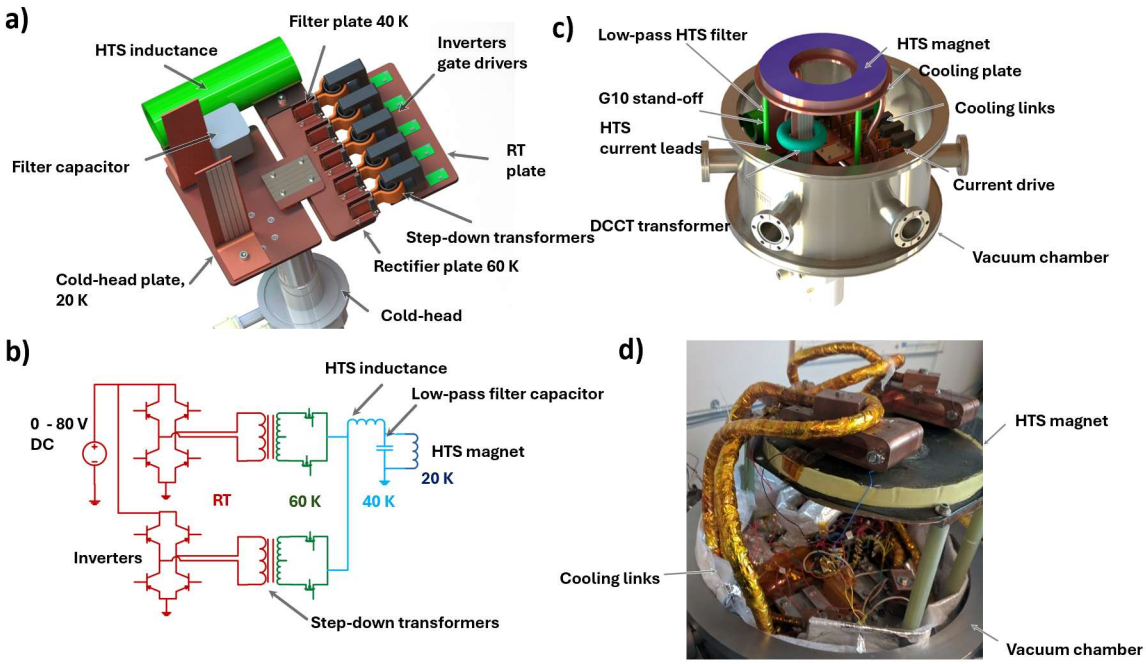

Fig. 2. a) Rendering of the current drive mechanical design. b) Simplified schematic of a single inverter-rectifier unit, schematically showing the temperature distribution within the unit. c) Placement of the current drive and the HTS magnet in an 18" cryo-chamber. d) Photograph of the experimental setup, showing the HTS coil and part of the vacuum chamber.

providing effective suppression of residual ripple at zero ohmic loss. The coil current is measured by a custom in-vacuum Direct DC Current Transformer (DCCT). We demonstrate that the in-vacuum, cryogenically cooled current source—schematically depicted in Fig. 1b—can achieve low voltage ripple and a thermal load comparable to that of a state-of-the-art conduction-cooled current lead.

II. EXPERIMENT

The source operates as a multi-stage synchronous rectifier. A DC voltage signal ranging from 0 to 80 V, up to 1 A, was transmitted into the cryogenic environment via a vacuum feedthrough. Voltage amplitude is regulated by a computer using feedback from the DCCT to maintain a stable coil current.

Each rectifier bridge contains six silicon MOSFETs (Vishay SQJA26EP), with channel resistance values of 1 mΩ at 20 °C and 0.5 mΩ at 77 K. Optimal performance was observed at 65 K.

The current source components were thermally attached to copper blocks measuring 6 mm in thickness, hereafter referred to as "plates" (see Fig. 2a). The gate drivers, cores and the primary windings of the transformers were interfaced with the designated "room temperature plate," which was mechanically bonded to the vacuum chamber via a copper braid of 10 mm diameter. This braid ensured thermal conduction from the transformer core and primary windings to the vacuum chamber wall.

The step-down transformers were made in-house by winding 100 turns of 24-gauge copper wire around a U-shaped ferromagnetic core (UR70/33/17 FerroxCube Mn-Zn ferrite). The secondary winding, configured as a so-called central-tapped winding, was comprised of two opposing turns of braids made of 60 strands of 24-gauge wire. The central tap of the windings was attached to a filter plate, which was also connected to a superconducting ripple filter. The secondary windings were bonded to the drain leads of the rectifying MOSFETS, three in parallel. The source terminals of the rectifying MOSFETS were attached to the filter plate, which was one of the current source terminals. The other source terminal was the filter solenoid; a filtering capacitor 470 µF (Metallized Polypropylene Film Capacitor, MKP-series, Vishay) was connected between the solenoid terminal and the ground. The source terminals of the rectifying MOSFETs were attached to a rectifier plate, which is connected to the cold head by a thermal bridge. The thermal bridge dimensions are chosen so that at the maximum current, 1,000 A, the rectifier is at the optimum temperature, 65 K. The AC power to step-down transformers was provided by a custom inverter based on an integrated full IGBT H-bridge (Microsemi Corporation). The rectifiers and inverters were controlled by an ARM Cortex-M7 controller, using a control algorithm proposed by Oomen *et al*. [9]. Briefly, the algorithm delays the closing of the rectifying MOSFETS to allow for the discharge of the parasitic leakage inductance of the step-down transformers. The current source powered a 120-turn, 0.15 mH double-pancake coil wound from 10 mm wide second-generation tape (Amperium, AMSC Corp.).

Fig. 2a illustrates the physical layout of the 700 A current drive. The transformer core and its primary winding were vacuum-potted using Stycast 2850FT, a thermally conductive epoxy. For cooling, a strap made of two 6 mm braided copper cables

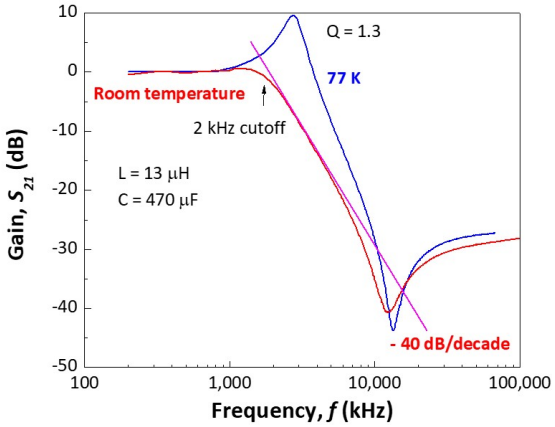

Fig. 3. The acceptance curve of the superconducting low-pass ripple filter at room temperature and 77 K.

was affixed to the transformer core, allowing heat to dissipate to the ambient environment via conduction through the vacuum chamber wall. Fig. 2b is a simplified schematic of the current drive. The schematic illustrates the temperature distribution within the unit when operating at a current of 700 A. For simplicity, only two rectifier modules are depicted in Fig. 2b, although the experiment utilized five modules connected in parallel to supply the current.

Fig. 2c presents a rendering and a photograph, Fig. 2d, of the complete test setup. The current source and the coil were housed inside an 18-inch vacuum chamber, equipped with a Cryomech single-stage cryopump mounted to the bottom flange. The superconducting coil was positioned above the rectifier, supported by 20 cm high G10 standoffs. This vertical separation was essential to prevent the coil's stray magnetic field from saturating the step-down transformer cores. To study the correlation between cold plate temperature and power dissipation, a 50 W resistive heater was installed on the rectifier plate.

The filter solenoid was wound from a stack of eight exfoliated filaments, each 2 mm wide, as previously outlined in [11]. A total of 25 turns were wound in a single layer, yielding a target inductance of 15 µH. Prior to winding, the tapes were pre-tinned with Sn63Pb37 solder, forming a solder layer approximately 10 µm thick. During the winding process, a 400 °C hot air stream was applied to the tape stack, instantly melting the solder and bonding the filaments together. Once winding was complete, the magnet was impregnated with thermally conductive Stycast 2850FT epoxy.

III. Results And Discussion

Fig. 3 presents the unloaded filter response measured at room temperature and at 77 K. The solenoid exhibits an inductance of 13 µH. In conjunction with a cryocooled 470 µF Polyesther film capacitor, the assembly is a second-order low-pass filter with a calculated cutoff frequency of approximately 2 kHz. At ambient conditions, the filter demonstrates optimal damping characteristics, whereas at cryogenic temperature (77 K), the response becomes overdamped, as indicated by a measured quality factor of Q = 1.3.

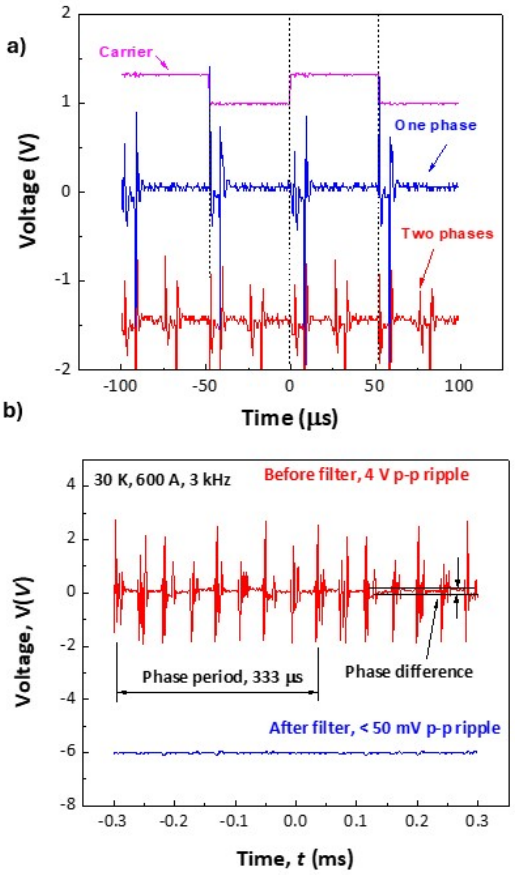

Fig. 4. a) Effect of phase activation on ripple voltage frequency. When two inverter phases are engaged, the ripple frequency is observed to double from 10 kHz to 20 kHz, demonstrating constructive phasing behavior. b) Comparison of the supply voltage waveform before and after superconducting filtering, recorded at a coil current of 600 A, filter temperature of 30 K, and inverter carrier frequency of 3 kHz. The post-filter waveform exhibits significant attenuation of high-frequency components.

The current source developed in this study comprises five independently addressable phases, as illustrated in Fig. 2, each phase switched following the algorithm described in [9]. Each phase is digitally switchable, allowing dynamic control over the current output. Fig. 4a illustrates a key performance advantage of the multi-phase current source architecture—namely, the multiplication of voltage ripple frequency. In this figure, the carrier frequency waveform is superimposed on the alternating component of the source voltage. When two phases are activated, the observed ripple frequency increases from 10 kHz to 20 kHz.

Fig. 4b illustrates the operational performance of the superconducting filter under a direct current load of 600 A with the inverter operating at 3 kHz, 30 K, five phases activated. Prior to filtering, the source exhibits a ripple voltage of approximately 4 V peak-to-peak. Post-filtering, the ripple voltage is significantly attenuated to approximately 20 mV peak-to-peak, demonstrating the filter's ability to suppress high-frequency noise. We note, however, variability among the transformers and rectifiers introduces a residual voltage ripple at the carrier frequency, which in this configuration is 3 kHz. To mitigate this effect, the filter was intentionally designed with

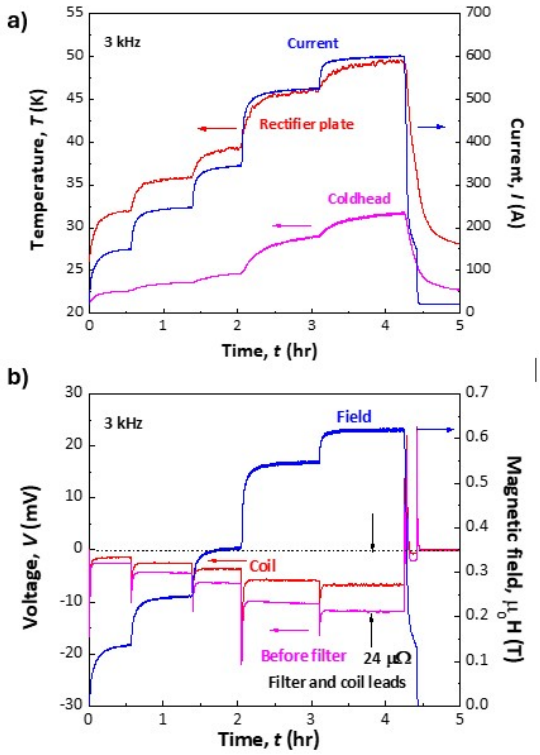

Fig. 5. a) Temperature evolution of the cold head and rectifier plate in response to a coil current ramp to 600 A under 3 kHz inverter operation. The data illustrate progressive heating of both components during the current ramp sequence. b). Time profiles of coil voltage and magnetic field corresponding to the ramping sequence shown in panel (a).

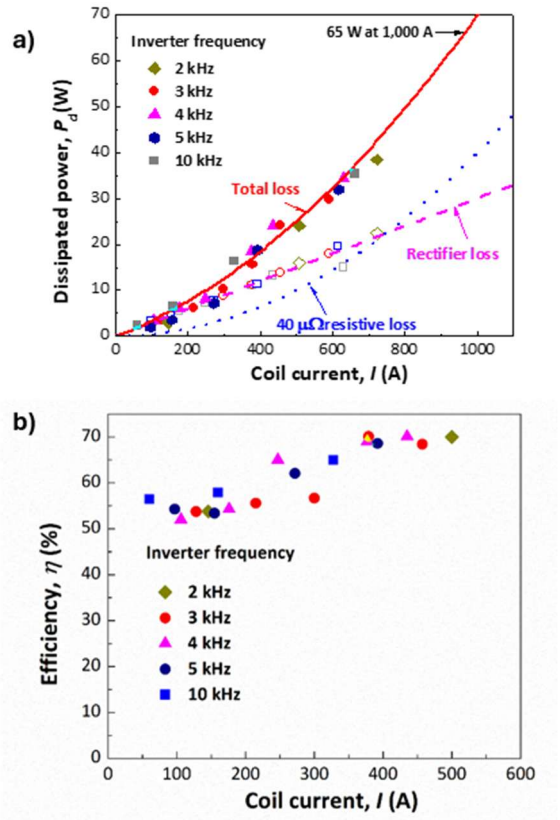

Fig. 6. a) Total power loss and rectifier-specific loss as functions of coil current. The solid curve represents a best-fit approximation of the total loss, modeled as the sum of linearly scaling rectifier loss and a resistive loss proportional to I^2. The dotted curve isolates the resistive loss component by subtracting the rectifier contribution from the total measured loss. b) Dependence of current source efficiency on inverter switching frequency. The data demonstrate a weak frequency sensitivity, consistent with conduction-dominated dissipation mechanisms.

a cutoff frequency below the inverter–rectifier array's carrier frequency, thereby enhancing suppression of the 3 kHz ripple component, see Fig. 3.

Fig. 5a depicts the time profile of the cold head and rectifier plate temperatures as the coil current is incrementally increased to 600 A. In parallel, Fig. 5b presents the corresponding profiles of the coil voltage and the voltage measured upstream of the AC filter during the same current ramp sequence. The coil current was raised in discrete steps, reaching a peak value of 600 A, at which point the coil generated a magnetic field of approximately 0.62 T at its center. Analysis of the voltage data allows estimation of the combined electrical resistance of the coil, current leads, and superconducting filter at full current, yielding a value of approximately 20 μΩ. During a subsequent ramp to 700 A, the rectifier plate temperature rose to 50 K, staying within the optimum temperature range for a Si MOSFET.

Fig. 6a summarizes the power loss components across five inverter switching frequencies, as inferred from current ramp data analogous to that presented in Fig. 5. The solid line represents a best-fit model characterizing the total loss as a combination of rectifier dissipation and an approximately quadratic ohmic contribution (I^2) of the passive circuit elements. The dashed line represents the rectifier-specific loss, exhibiting a linear dependence on current. This approximation enables estimation of the total ohmic contribution to the thermal load, yielding a value of approximately 40 μΩ.

Fig. 6b provides a comparative assessment of current source efficiency at switching frequencies of 2, 3, 4, 5, and 10 kHz. Efficiency is defined as the ratio of power delivered from the room-temperature high-voltage supply to the power dissipated at the cryogenic end during steady-state magnet operation

The weak frequency dependence of the loss, Fig. 6b, suggests that conduction is the dominant dissipation mechanism, and switching and AC losses are minor contributors. Resistive loss in passive components, 40μΩ total, accounts for approximately 50% of the total dissipation, where 40% is the resistivity of current leads and the filter, and the rest is the resistance of the secondary winding and other copper connections. The resistive dissipation can be significantly reduced by soldering 2G tapes of the copper components, thus effectively shunting them. The rectifier loss is projected to account for 15 W of heat load at 1,000 A. This source of heat can only be further reduced by the parallel connection of more rectifying MOSFETs and using elements with lower channel resistance. For example, a flux pump reported by Jurco *et al.* [10], used 12 parallel switching MOSFETS and demonstrated approximately 4 W of dissipation at 700 A, 77 K. The new n-channel devices that use U-MOS technology offered by Toshiba claim a typical room

temperature channel resistance of 300 μΩ, which is 40% lower than devices used in this study. We estimate that combining shunted copper components with an improved rectifier can reduce the total heat load below 10 W at 1,000 A per pair of leads.

The benefits of a MOSFET-based rectifier are only achieved if the body diode does not conduct. If the MOSFET closes before secondary leakage inductance is discharged, the body diode activates, adding about 37 W heat at 500 A due to its >1 V forward voltage at 77 K. To prevent this switching loss, closing of the rectifying switch is delayed relative to the secondary voltage, as suggested by Oomen et al. [9]. However, this delay also restricts source frequency; the delay time cannot exceed half the inverter period. Thus, increasing current requires more small rectifier-inverter phases rather than scaling up the transformer and rectifier. This is because $\times n$ larger transformer will have proportionally larger leakage inductance and $\times n$ higher secondary current, resulting in $\times n^2$ longer discharge time and $1/n^2$ lower operation frequency. Such a current source will be very bulky and generate low-frequency ripple, which would be difficult to filter. A higher current source of the proposed design would use more inverter-rectifying units (see Fig. 2), thus maintaining the switching frequency > 3 kHz and keeping the system compact.

Although current high-temperature superconducting (HTS) magnets typically employ a no-insulation configuration and thus rely on passive quench protection mechanisms [12], active quench protection schemes involving energy extraction may be required for fast-cycling magnet applications. If implemented, such schemes would necessitate that the current source survives voltages exceeding 1 kV. In the present study, the filtering capacitor and rectifying MOSFETs are rated for breakdown voltages of approximately 50 V. Advanced high-voltage components, such as gallium nitride devices, are compatible with cryogenic operation [13] and offer a potential pathway for constructing current sources capable of supporting the active quench management.

IV. Conclusion

In conclusion, a cryogenic in-vacuum synchronous rectifier with a superconducting second-order ripple filter was used to power a conduction-cooled superconducting coil which generated 0.6 T at 30 K. The current source dissipated 35 W of heat at 700 A, 30 K. The proposed design combines several desirable features, such as modularity, compact shape and utilization of off-the-shelf inexpensive components, except for the superconducting filter.

References

[1] A. Ballarino, "Current leads for the LHC magnet system," *IEEE Trans. Appl. Supercond.,* vol. 12, no. 1, pp. 1275-1280, Mar 2002, doi: 10.1109/tasc.2002.1018635.

[2] R. McFee, "Optimum Input Leads for Cryogenic Apparatus," *Rev. Sci. Instrum.,* vol. 30, no. 2, pp. 98-102, 1959, doi: 10.1063/1.1716499.

[3] S. Zhang, H. Feng, M. Zhuang, K. Ding, C. Liu, and Y. Zhou, "Experimental Research of a 10 kA HTS Current Lead Using YBCO Tapes," *IEEE Trans. Appl. Supercond.,* vol. 30, no. 8, pp. 1-7, 2020, doi: 10.1109/TASC.2020.3004542.

[4] R. Heller, W. H. Fietz, F. Gröner, M. Heiduk, M. Hollik, C. Lange, and R. Lietzow, "Test results of a 20 kA high temperature superconductor current lead using RE BCO tapes," *Supercond. Sci. Technol.,* vol. 31, no. 5, p. 055014, 2018. [Online]. Available: http://stacks.iop.org/0953-2048/31/i=5/a=055014.

[5] V. Fry, A. Zhukovsky, M. J. Wolf, P. C. Michael, R. F. Vieira, W. K. Beck, R. Barnett, J. Estrada, E. Ihloff, C. Vidal, T. Golfinopoulos, and Z. S. Hartwig, "50-kA Capacity, Nitrogen-Cooled, Demountable Current Leads for the SPARC Toroidal Field Model Coil," *IEEE Trans. Appl. Supercond.,* vol. 34, no. 2, pp. 1-18, 2024, doi: 10.1109/TASC.2024.3354237.

[6] C. W. Bumby, R. A. Badcock, H.-J. Sung, K.-M. Kim, Z. Jiang, A. E. Pantoja, P. Bernardo, M. Park, and R. G. Buckley, "Development of a brushless HTS exciter for a 10 kW HTS synchronous generator," *Supercond. Sci. Technol.,* vol. 29, no. 2, p. 024008, 2016/01/12 2016, doi: 10.1088/0953-2048/29/2/024008.

[7] T. A. Coombs, J. Geng, L. Fu, and K. Matsuda, "An Overview of Flux Pumps for HTS Coils," *IEEE Trans. Appl. Supercond.,* vol. 27, no. 4, pp. 1-6, 2017, doi: 10.1109/TASC.2016.2645130.

[8] O. Mueller, "On-resistance, thermal resistance and reverse recovery time of power MOSFETs at 77 K," *Cryogenics,* vol. 29, no. 10, pp. 1006-1014, 1989/10/01/ 1989, doi: https://doi.org/10.1016/0011-2275(89)90250-6.

[9] M. P. Oomen, M. Leghissa, G. Ries, N. Proelss, H. Neumueller, F. Steinmeyer, M. Vester, and F. Davies, "HTS flux pump for cryogen-free HTS magnets," *IEEE Trans. Appl. Supercond.,* vol. 15, no. 2, pp. 1465-1468, 2005, doi: 10.1109/TASC.2005.849129.

[10] R. Jurčo, A. Vaskuri, B. Curé, A. Dudarev, and M. Mentink, "MOSFET-based HTS flux pump," *Supercond. Sci. Technol.,* vol. 36, no. 11, p. 115025, 2023/10/09 2023, doi: 10.1088/1361-6668/acfbfc.

[11] V. Solovyov, Z. Mendleson, and M. Takayasu, "Defect Tolerant High-Temperature Superconducting Cable for the Central Solenoid of Compact Fusion Reactor," *IEEE Trans. Appl. Supercond.,* vol. 31, no. 5, pp. 1-5, 2021, doi: 10.1109/TASC.2021.3052444.

[12] Y. Wang, W. K. Chan, and J. Schwartz, "Self-protection mechanisms in no-insulation (RE)Ba2Cu3Ox high temperature superconductor pancake coils," *Supercond. Sci. Technol.,* vol. 29, no. 4, p. 045007, 2016/03/03 2016, doi: 10.1088/0953-2048/29/4/045007.

[13] H. Mustafeez ul, A. I. Emon, F. Luo, and V. Solovyov, "Design and Validation of a 20 kVA, Fully Cryogenic, 2-Level GaN Based Current Source Inverter for Full Electric Aircrafts," *IEEE Transactions on Transportation Electrification,* vol. 8, no. 4, pp. 4743-4759, Dec. 2022, doi: 10.1109/TTE.2022.3176842.